Differences in hemispherical thalamo-cortical causality analysis during resting-state fMRI

Abdul Rauf Anwar[1*], Makii Muthalib [2], Stephane Perrey[3], Stephan Wolff[4], Günther Deuschl[5], Ulrich Heute[1], and Muthuraman Muthuraman[5]

***Abstract*— Thalamus is a very important part of the human brain. It has been reported to act as a relay for the messaging taking place between the cortical and sub-cortical regions of the brain. In the present study, we analyze the functional network between both hemispheres of the brain with the focus on thalamus. We used conditional Granger causality (CGC) and time-resolved partial directed coherence (tPDC) to investigate the functional connectivity. Results of CGC analysis revealed the asymmetry between connection strengths of the bilateral thalamus. Upon testing the functional connectivity of the default-mode network (DMN) at low-frequency fluctuations (LFF) and comparing coherence vectors using Spearman's rank correlation, we found that thalamus is a better source for the signals directed towards the contralateral regions of the brain, however, when thalamus acts as sink, it is a better sink for signals generated from ipsilateral regions of the brain.**

I. INTRODUCTION

One of the most interesting features of the human brain is that it is nearly always active. It has been reported that the difference between the amount of energy consumed by the brain during evoked tasks and during rest is minimal [1]. This fact makes the analysis of the brain at resting state almost as important as its analysis during some neuronal task. Discovery of default-mode network (DMN) paced the quest for better understanding of human brain at rest [2] [3]. Default-mode network is turned-off whenever the brain is subjected to carry out an evoked task. Parts of DMN include precuneus, pre-frontal cortex, medical pre-frontal cortex and parietal cortex [3]. Moreover, DMN is primarily characterized by low-frequency fluctuations (LFF), typically in the range of (0.01-0.1 Hz) [4]. These LFF are distinct from physiological artifacts like respiratory (0.1-0.5 Hz) and cardiac rhythms (0.6-1.2 Hz) [4].

Functional magnetic-resonance imaging (fMRI), introduced in 1990 by S. Ogawa, is one of the promising modalities to measure the brain activity [5]. Exploiting the magnetic properties of the Hydrogen atoms in human blood, fMRI is able to localize the brain activity even in the sub-cortical regions of the brain. However, fMRI has a very low temporal resolution. One deciding factor for the temporal resolution of fMRI is the repetition time (TR), the acquisition time between two successive fMRI volumes. Typically, fMRI has a TR of about 2 seconds. This means that fMRI can sample data roughly at around 0.5 Hz, and the ultimate resolveable maximum frequency in fMRI data will be half of the sampling rate according to the Nyquist criterion. Because of the low frequency range of LFF, these frequencies can be effectively analyzed using fMRI modality.

Nowadays, it is very vital to understand the causal functional networks within the brain. Various methods exist to analyze such causality within the brain. Methods like structural equation modeling (SEM), and dynamic causal modeling (DCM) have traditionally been applied to fMRI data for such directionality analysis [17]. Such methods, though being able to quantify causality at neuronal level, are always based on some a-priori assumptions about the anatomical networks [17]. This factor limits their application and interpretation of their results. The methods based on multivariate auto-regressive modeling (MVAR) are independent of any such presumption. They are reported to be a viable approach for causal analysis of the brain signals [6] [7].

II. METHODS

Multivariate auto-regressive modeling is based on modeling the subjected data with a set of auto-regressive (AR) equations. The employment of such models to time series can facilitate the application of causal analysis methods, i.e., Granger causality (GC). The principle behind causality is that, if the inclusion of past values of a first time series improves the estimation of the second time series, then the first time series is "Granger causing" the second time series [8] [9]. Mathematically, GC can be described by considering equation (1), where linear regression is used to estimate present value of time series x using its own past values:

$$x(t) = \sum_{j=1}^{p} a_1 x(t-j) + \epsilon_1(t). \quad (1)$$

Here, a_1 is the AR coefficient, and $\epsilon_1(t)$ is the residual noise. Moreover, the noise variance for the equation (1)

This work was supported by SFB 855 Project D2

[1]A. R. Anwar* and U. Heute are with Faculty of Electrical Engineering, Digital Signal Processing and System Theory, University of Kiel, 24143-Kiel, Germany. ara at tf.uni-kiel.de uh at tf.uni-kiel.de

[2]M. Muthalib is with Movement to Health (M2H), Euromov, Montpellier-1 University, 34090 Montpellier, France and also with the Faculty of Health, Queensland University of Technology, 4059-Brisbane, Australia. makii.muthalib at univ-montp1.fr

[3]S. Perrey is with Movement to Health (M2H), Euromov, Montpellier-1 University, 34090 Montpellier, France stephane.perrey at univ-montp1.fr

[4]S. Wolff is with the Department of Neuroradiology, University of Kiel, 24105-Kiel, Germany. s.wolff at neurorad.uni-kiel.de

[5]G. Deuschl and M. Muthuraman are with the Department of Neurology, Universitätsklinikum Schleswig-Holstein, 24105-Kiel, Germany. g.deuschl at neurologie.uni-kiel.de m.muthuraman at neurologie.uni-kiel.de

978-1-4244-7929-0/14/$26.00 ©2014 IEEE

above can be given as

$$\sigma^2_{Model_1} = \left[var(\epsilon_1(t))\right]. \quad (2)$$

Now we assume that, in the same model, we have an additional information as time series z. This additional time series is also contributing towards the estimation of time series x as given in equation (3) below, and vice-versa, as described in equation (4):

$$x(t) = \sum_{j=1}^{p} a_2 x(t-j) + \sum_{j=1}^{p} b_2 z(t-j) + \epsilon_2(t). \quad (3)$$

$$z(t) = \sum_{j=1}^{p} c_2 x(t-j) + \sum_{j=1}^{p} d_2 z(t-j) + \epsilon_3(t). \quad (4)$$

The corresponding variance and co-variance matrix for above model can be given as:

$$\sigma^2_{Model_2} = \begin{bmatrix} var(\epsilon_2(t)) & cov(\epsilon_2(t), \epsilon_3(t)) \\ cov(\epsilon_3(t), \epsilon_2(t)) & var(\epsilon_3(t)) \end{bmatrix}. \quad (5)$$

Now, if by inclusion of time series z the variance of error term $\epsilon(t)$ is reduced, than we say that time series z is "Granger causing" time series x. An empirical expression for the calculation of GC can be given as [9]

$$F_{z \to x} = \ln \left[\frac{var(\epsilon_1(t))}{var(\epsilon_2(t))} \right]. \quad (6)$$

Granger causality gives a scalar value, showing the extent of causality from one signal to the other signal. However, in biomedical-signal analysis, we are usually interested in signals corresponding to the certain frequencies, e.g., in the alpha frequency band (8-13 Hz). Time-resolved partial directed coherence (tPDC) is a method, based on multivariate auto-regressive modeling, that can quantify causal information between two signals corresponding to a certain frequency. In addition to this frequency information, tPDC also has the ability to show the time dynamics of such causal connections. A mathematical expression for tPDC can be derived by considering a general auto-regressive (AR) model with order p as follows:

$$x_i(t) = \sum_{r=1}^{r=p} a_{ij,r} x_j(t-r) + \epsilon(t). \quad (7)$$

Equation (7) refers to a stationary process, in which time series x_j is causing time series x_i; p is the model order, and a_{ij} are the causal coefficients that can be found by using techniques like Burg's method or Yule-Walker equations. After estimation of the causal coefficients they are transformed into the Fourier domain and their normalization yields the following expression of the partial directed coherence (PDC),

$$|\pi_{i \leftarrow j}(\omega)| = \frac{|A_{ij}(\omega)|}{\sqrt{\sum_k |A_{kj}(\omega)|^2}}. \quad (8)$$

In equation (8), $\pi_{i \leftarrow j}(\omega)$ is the magnitude of partial directed coherence from time series x_j to x_i at frequency ω. A_{ij} is the Fourier transform of the causal coefficients a_{ij}. Due to the above stationary assumption, the model coefficients a_{ij} do not evolve over the course of time; however, for non-stationary signals, such coefficients have to be time-varying and their estimation should be updated regularly. One way of estimating time-varying coefficients is by using a *dual-extended Kalman filter* (DEKF). After estimation of coefficients, PDC is calculated at each time and finally all PDC coherence vectors are concatenated to give a time-frequency plot of tPDC. Further details about the implementation of DEKF can be found elsewhere [8]. One important factor is to determine, how many coefficients will be sufficient to describe the AR model of the subjected time series. Algorithms such as, Akaike's information criterion (AIC) or the Bayesian information criterion (BIC) can be used to determine the optimum model order. Empirically, AIC, which is based on minimizing Kullback-Leibler information entropy between fitted mode and observed data, can be described by the expression [10] as

$$AIC = -2 \ln \mathcal{L}_{max} + 2k. \quad (9)$$

In equation (9), $\mathcal{L}_{max}$ is the maximum likelihood of the model and k is the number of parameters in the fitted model. In the present study AIC was used to estimate the optimum model order.

III. Data Acquisition

Resting state fMRI was recorded from 11 healthy subjects (Mean age 25 years, four males) for 10 minutes. BOLD-sensitive MRI was performed with a 3-Tesla MR scanner (Philips, the Netherlands). A single-shot T1-weighted, gradient-echo planar imaging sequence was used for fMRI (TR = 2500 ms, TE = 45 ms, 32 slices, 64 x 64 matrix, slice thickness = 3.5 mm, FOV = 200 mm, flip angle = 90). A total of 240 fMRI volumes were acquired in 10 minutes.
All fMRI volumes were re-aligned to the very first volume of recording to remove any motion artifacts occurred during the course of recording. Moreover, the volumes were also normalized to bring all volumes in standard subspace by minimizing the sum of square differences between volumes to be normalized and the standard template image. Finally, smoothing was performed by convolving all volumes with a Gaussian kernel of full width at half maximum (FWHM) to suppress noise. No temporal pre-processing was performed for fMRI volumes except discarding the first 10 recorded volumes to allow for magnetic saturation effects. All pre-processing was performed using SPM08 toolbox (http://www.fil.ion.ucl.ac.uk/spm). Afterwards using toolbox of "Data preprocessing assistant for resting state fMRI advanced" (DPARSFA), we extracted time courses from 10 regions of the brain, namely, bi-lateral parietal cortex, precuneus, prefrontal cortex, medial frontal cortex, and thalamus [15] [16]. Details about the MNI coordinates of all these regions are given in Table I.

In order to extract the time courses, spheres with radius of 7mm was assumed at these MNI coordinates, and local maximum was found using a custom code in MATLAB. Afterwards, this maximum is considered as center of a sphere

TABLE I

MNI COORDINATES OF BRAIN REGIONS ON BOTH LEFT AND RIGHT HEMISPHERE OF THE BRAIN.

Region	Left (MNI)	Right (MNI)
Parietal	30, -60, 57	-31, -58, 57
Prefrontal	32, 37, 39	-34, 37, 39
Medial frontal cortex	7, 58, 21	-6, 59, 21
Thalamus	10, -40, -14	-18, -40, -14
Precuneus	21, -62, 14	-19, -62, 14

with radius 3mm and time series were extracted from this sphere using DPARSFA. The temporal mean of the time series was removed and they were de-trended. The optimum model order was estimated and conditional Granger causality was applied to two sets of five time series (both left and right hemisphere of the brain separately). The optimum model order was fixed for all subjects; moreover, consistency of the applied model was tested by comparing the correlation structures of the actual data and the simulated data with similar parameters. A toolbox for Granger-causalality connectivity analysis was used for calculation of conditional Granger causality (CGC) [11]. Moreover, as a test of significance, Bonferroni correction was applied to CGC values. After conditional-Granger causality analysis, time-resolved partial directed coherence (tPDC) was applied on five time series from each hemispheres separately. Low-frequency fluctuations (LFF) (0.01-0.1 Hz) were taken as reference frequency band and coherence time-dynamics vectors corresponding to LFF were extracted for each connection from both left and right hemispheres. The LFF band is not affected by the physiological artifacts. The vectors from both hemispheres were compared to each other using Spearman's rank correlation to see whether the dynamics in each hemisphere are similar or not. The Spearman's rank correlation was chosen because the data came from a non-Gaussian distribution.

IV. RESULTS

For the CGC analysis of resting state fMRI, we focused on thalamus and took it as a main node and analyzed the connectivity network with reference to it. We did this owing to the significance of thalamus in the brain. We took the mean of the connection strengths of the regions of the brain which lie at the rear part of the head, i.e., parietal and precuneus, and termed it as 'back'; and also for frontal regions, i.e., prefrontal and medial frontal cortex, and termed it as 'front'. Analysis of CGC on these three regions of the brain yielded the functional network as shown in Fig. 1.

The causality network as revealed in Fig. 1. shows that all regions of the brain have bi-directional connections with the thalamus in their respective hemispheres. To further quantify this observation, we took the mean of all the CGC connections going to and coming from thalamus in both left and right hemispheres. The values are shown in Table II.

As we can see now, there is a difference in the symmetry of the connections coming out and going towards thalamus in the right and left hemisphere. In the right hemisphere, the strength of connections coming from thalamus is large

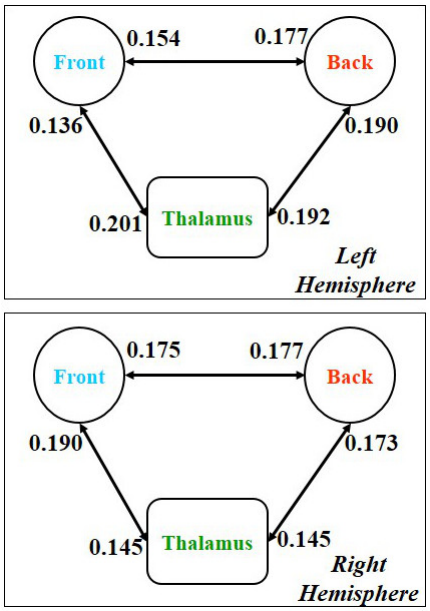

Fig. 1. Conditional Granger causality results for both hemispheres. Bi-directional connections exist between thalamus and other cortical regions. Asymmetry between strength of connections going to and coming from thalamus between left and right thalamus can also be seen.

TABLE II

AVERAGE CONNECTION STRENGTH OF CONNECTIONS ORIGINATING AND TERMINATING AT THALAMUS IN BOTH HEMISPHERES.

	Left Hemisphere	Right Hemisphere
From Thalamus	0.163	0.1815
To Thalamus	0.1965	0.145
Overall connection strength	0.175	0.1675

than those of going towards thalamus. However, in left hemisphere the strength of connections going towards thalamus is large than that of coming out of thalamus. Afterwards we applied tPDC on five time series within each hemisphere. We extracted the coherence vectors from the time-frequency plot of tPDC corresponding to the LFF frequency band. The connections in each hemisphere were compared using Spearman's rank correlation. Within each hemisphere, the highest number of positive significant correlations was observed when thalamus acts as a sink for all the connections originating from all ipsilateral regions. However, when thalamus is considered as a source, then smaller number of positive correlations was observed between thalamus and the ipsilateral regions of the hemisphere. Afterwards we replaced the thalamus in each hemisphere with the contralateral thalamus. Now large number of positive correlations was observed when thalamus acts as a source of connections for all contralateral regions of the brain. The smaller number of positive correlations was observed when thalamus was considered as sink of the signals from contralateral regions of the brain. For Spearman's rank correlation, the p-value was set to 0.05. All nodes in the left hemisphere except thalamus are termed left cortex, and all nodes in the right hemisphere are termed right cortex. Blue lines in Fig. 2. show

the high number of positive significant correlations, meaning time dynamics of tPDC vector on either side, between same connections, of the brain are similar; however, pink lines show a low number of positive significant correlations, showing dissimilar time dynamics of tPDC vectors.

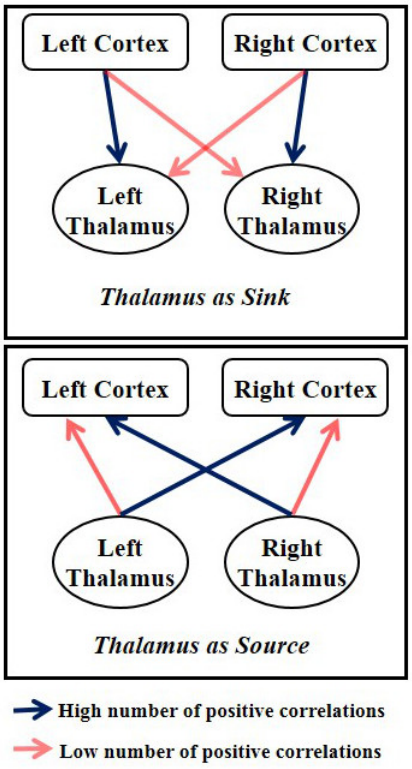

Fig. 2. Number of positive correlations between coherence vectors in left and right hemisphere. Thalamus is better sink for ipsilateral regions and better source for contralateral regions of the brain.

V. CONCLUSIONS

In our study we analyzed the causality in resting-state fMRI data with focus on thalamus. For simple causality, we used conditional Granger causality and observed the asymmetry between left and right hemispheres. The method CGC quantifies the causality by one scalar value showing the strength of connection. The tPDC method, however, can reveal the frequency and time dynamics of causal networks. Hence by using the tPDC we can overcome the limitation of CGC and analyze the DMN at the LFF frequency band. Results show that thalamus is a better sink for the connections originating from the ipsilateral regions of the brain. However, when thalamus works as a source, it is a better source for contralateral regions of the brain. Such asymmetry between thalamo-cortical connections could be due to the difference in number of neurons and volume between bilateral thalamus [12]. Moreover, previous studies have shown that the visual cortex, at least, has dissimilar connectivity with both thalamus of the brain [13]. Due to the difference in anatomy of human brain, thalamus is is reported to have predominantly ipsilateral cortical connections [14], which is in line with our results where thalamus acts as source of connection. However, in order to better understand the functional significance of thalamus, further analyses need to be undertaken.

ACKNOWLEDGMENT

Support from the German Research Council (Deutsche Forschungs Gemeinschaft, DFG, SFB 855, Project D2) is gratefully acknowledged.

REFERENCES

[1] M. E. Raichle, A. Z. Snyder, A default mode of brain function: A brief history of an evolving idea, NeuroImage, vol. 37, no. 4, pp. 1083 - 1090, 2007.
[2] M. E. Raichle, A. M. Macleod, A. Z. Snyder, W. J. Powers, A. D. Gusnard, G. L. Shulman, A default mode of brain function, Proceedings of the National Academy of Sciences, vol. 98, no. 2, pp. 676-682, 2001.
[3] G. G. Knyazev, J. Y. Slobodskoj-Plusnin, A. V. Bocharov, L. V. Pylkova, The default mode network and EEG alpha oscillations: An independent component analysis, Brain Research, vol. 1402, no. 0, pp. 67 - 79, 2011.
[4] D. M. Cole, S. M. Smith, C. F. Beckmann, Advances and pitfalls in the analysis and interpretation of resting-state FMRI data, Frontiers in Systems Neuroscience, vol. 4, no. 8, pp. , 2010.
[5] S. Ogawa, T. M. Lee, A. R. Kay, D. W. Tank, Brain magnetic resonance imaging with contrast dependent on blood oxygenation., Proceedings of the National Academy of Sciences of the United States of America, vol. 87, no. 24, pp. 9868 - 9872, 1990.
[6] A. K. Seth, P. Chorley, L. C. Barnett, Granger causality analysis of fMRI BOLD signals is invariant to hemodynamic convolution but not downsampling, NeuroImage, vol. 65, no. 0, pp. 540 - 555, 2013.
[7] X. Wen, G. Rangarajan, M. Ding, Is Granger causality a viable technique for analyzing fMRI data?, PLoS ONE, vol. 8, no. 7, e67428, 2013.
[8] A. R. Anwar, M. Muthalib, S. Perrey, A. Galka, O. Granert, S. Wolff, G. Deuschl, J. Raethjen, U. Heute, M. Muthuraman, Comparison of causality analysis on simultaneously measured fMRI and NIRS signals during motor tasks, Engineering in Medicine and Biology Society (EMBC), 2013 35th Annual International Conference of the IEEE , vol., no., pp.2628-2631, 3-7 July 2013.
[9] A. R. Anwar, M. Muthalib, S. Perrey, A. Galka, O. Granert, S. Wolff, G. Deuschl, J. Raethjen, U. Heute, M. Muthuraman, Directionality analysis on functional magnetic resonance imaging during motor task using Granger Causality, Engineering in Medicine and Biology Society (EMBC), 2012 34th Annual International Conference of the IEEE , vol., no., pp.2287-2290, August 2012.
[10] A. R. Liddle, Information criteria for astrophysical model selection, Monthly Notices of the Royal Astronomical Society: letters , vol. 377, no. 1, pp.L74-L78, 2007.
[11] A. K. Seth, A MATLAB toolbox for Granger causal connectivity analysis, J Neurosci Methods , vol. 186, no. 2, pp. 262-273, 2010.
[12] M. Corbetta, F. M. Miezin, S. Dobmeyer, G. L. Shulman, S. E. Peterson, Selective and divided attention during visual discriminations of shape, color, and speed: Functional anatomy by positron emission tomography, J Neurosci., vol. 11, no., pp. 2383-2402, 1991.
[13] Q. Zou, X. Long, X. Zou, C. Yan, C. Zhu, Y. Yang, D. Liu, Y. He, Y. Zang, Functional connectivity between the thalamus and visual cortex under eyes closed and eyes open conditions: A resting-state fMRI study, Hum Brain Mapp, vol. 30, no. 9, pp. 3066-3078, 2009.
[14] G. A. Ojemann, Asymmetric function of the thalamus in man, Annals of the New York Academy of Sciences, vol. 299, no. 1, pp. 380–396, 1977.
[15] Y. Chao-Gan, Z. Yu-Feng, DPARSF: a MATLAB toolbox for “pipeline data” analysis of resting-state fMRI, Front. Syst. Neurosci., vol. 4, no. 13, pp. , 2010.
[16] X-W. Song, Z-Y. Dong, X-Y. Long, S-F. Li, X-N. Zuo, C-Z. Zhu, Y. He, C-G. Yan, Y-F. Zang, REST: A Toolkit for resting-state functional magnetic tesonance imaging data processing, PLoS ONE, vol. 6, no. 9, e25031, 2011.
[17] K. E. Stephen, K. j. Friston, Analyzing effective connectivity with fMRI, Wiley Interdiscip Rev Cogn Sci., vol. 1, no. 3, pp. 446-459 , 2010.